Inorg. Chem. **2007**, *46*, 1401−1409

Integrated Experimental−Theoretical Investigation of the Na−Li−Al−H System

Susanne M. Opalka,*,† Ole M. Løvvik,‡,§ Hendrik W. Brinks,§ Paul W. Saxe,£ and Bjørn C. Hauback§

United Technologies Research Center, East Hartford, Connecticut 06108, Centre for Materials Science and Nanotechnology, University of Oslo, N-0318 Oslo, Norway, Institute for Energy Technology, P.O. Box 24 N-2027 Kjeller, Norway, and Materials Design, Inc., Angel Fire, New Mexico 87710

Received October 23, 2006

First-principles modeling, experimental, and thermodynamic methodologies were integrated to facilitate a fundamentally guided investigation of quaternary complex hydride compounds within the bialkali Na–Li–Al–H hydrogen storage system. The integrated approach has broad utility for the discovery, understanding, and optimization of solid-state chemical systems. Density functional theory ground-state minimizations, low-temperature powder neutron diffraction, and low-temperature synchrotron X-ray diffraction were coupled to refine the crystallographic structures for various low-temperature distorted Na_2LiAlH_6 allotropes. Direct method lattice dynamics were used to identify a stable Na_2LiAlH_6 allotrope for thermodynamic property predictions. The results were interpreted to propose transformation pathways between this allotrope and the less stable cubic allotrope observed at room temperature. The calculated bialkali dissociation pressure relationships were compared with those determined from pressure-composition-isotherm experiments to validate the predicted thermodynamic properties. These predictions enabled computational thermodynamic modeling of Na_2LiAlH_6 and competing lower order phases within the Na–Li–Al–H system over a wide of temperature and pressure conditions. The predictions were substantiated by experimental observations of varying Na_2LiAlH_6 dehydrogenation behavior with temperature. The modeling was used to identify the most favorable reaction pathways and equilibrium products for H discharge/recharge in the Na–Li–Al–H system, and to design conditions that maximize the theoretical hydrogen reversibility within the Na–Li–Al–H system.

Introduction

This study will illustrate the utility of combining first-principles, experimental, and thermodynamic methodologies to tune the reversible hydrogen capacity within the Na−Li−Al−H compositional system. This integration of methodologies was inspired by the need to develop high capacity hydrogen storage media; however, the approach described herein is broadly applicable toward the discovery of new solid-state compounds and the investigation of their behavior. A quaternary phase within this system, Na_2LiAlH_6, has been the subject of a number of recent studies in the hydrogen storage community.[1−6] A major motivation for studies of the Na−Li−Al−H system was the prospect of developing a mixed bialkali alanate phase that leveraged both the reversibility of the sodium alanates and the higher capacity of the lithium alanates.[4−10] This rationale is evident from a van't Hoff plot of the equilibrium sodium and lithium alanate dissociation pressures constructed from recent thermody-

* E-mail: opalkasm@utrc.utc.com.
† United Technologies Research Center.
‡ University of Oslo.
§ Institute for Energy Technology.
£ Materials Design, Inc.

(1) Bogdanovic, B.; Schwickardi, M. *J. Alloys Comp.* **1997**, *253*−*254*, 1−9.
(2) Hout, J.; Boily, S.; Guther, V.; Schulz, R. *J. Alloys Comp.* **1999**, *283*, 304−306.
(3) Brinks, H. W.; Hauback, B. C.; Jensen, C. M.; Zidan, R. *J. Alloys Comp.* **2005**, *392*, 27−30.
(4) Fossdal, A.; Brinks, H. W.; Fonneløp, J. E.; Hauback, B. C. *J. Alloys Comp.* **2005**, *397*, 135−139.
(5) Graetz, J.; Lee, Y.; Reilly, J. J.; Park, S.; Vogt, T. *Phys. Rev. B* **2005**, *71*, 1844115/1−7.
(6) Nakamura, Y.; Fossdal, A.; Brinks, H. W.; Hauback, B. C. *J. Alloys Comp.* **2006**, *416*, 274−278.
(7) Arroyo y de Dompablo, M. E.; Ceder, G. *J. Alloys Comp.* **2004**, *364*, 6−12.
(8) Løvvik, O. M.; Swang, O. *Europhys. Lett.* **2004**, *67*, 607−613.
(9) Løvvik, O. M.; Swang, O. *J. Alloys Comp.* **2005**, *404*−*406*, 757−761.
(10) Løvvik, O. M.; Swang, O.; Opalka, S. M. *J. Mater. Res.* **2005**, *20*, 3199−3213.

10.1021/ic062032e CCC: $37.00
Published on Web 01/20/2007

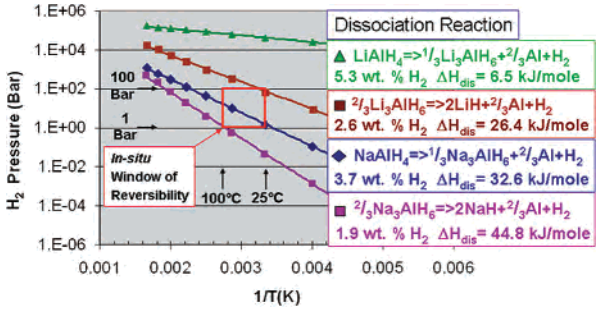

Figure 1. The van't Hoff plot predicted for the first and second dissociation reactions of lithium and sodium alanate. The wt. % H_2 discharged and the dissociation enthalpy, ΔH_{dis}, are listed for each reaction (from refs 11 and 12).

namic predictions[11,12] in Figure 1. The practical operating 1−100 bar pressure range and 25−100 °C temperature range for hydrogen storage reversible dehydrogenation and rehydrogenation on-board of a transportation vehicle was used to define an "in situ window of reversibility" in the plot. In the first reaction of the sodium alanate system, sodium aluminum tetrahydride, $NaAlH_4$, dissociates to release 3.7 wt. % molecular hydrogen, H_2. The predicted equilibrium dissociation pressure of this reaction traverses the in situ window of reversibility. However, the predicted equilibrium pressure for second sodium alanate dissociation reaction skims the lower left corner of the window of reversibility. Here, the more stable trisodium aluminum hexahydride, Na_3AlH_6, dissociates to release an additional 1.9 wt. % H_2. Since both reactions are only partially reversible in Ti-activated sodium alanate in practice,[12,13] the sodium alanate system does not meet the DOE 2006 hydrogen storage gravimetric target of 4.5 wt. % H_2. The lithium alanate system has a greater H_2 gravimetric capacity. In the first and second dissociation reactions given in Figure 1, lithium aluminum tetrahydride, $LiAlH_4$, and trilithium aluminum hexahydride, Li_3AlH_6, dissociate to release 5.3 and 2.6 wt. % H_2, respectively. However, as shown in Figure 1, the predicted dissociation pressures of these less stable reactions lie inaccessibly above the in situ window of reversibility. Recent modeling investigations exploring the possible increase in gravimetric capacity of the sodium alanates through lithium substitution on the sodium sublattice, or the possible lowering of the lithium alanates' dissociation pressure through sodium substitution on the lithium sublattice, predicted that Na_2LiAlH_6 is the sole stable phase in the Na−Li−Al−H quaternary system.[8−10] On the basis of these findings, integrated theoretical-experimental methodologies were used in this study to design the maximum theoretical hydrogen storage capacity that could be achieved with this Na_2LiAlH_6 phase within the Na−Li−Al−H system.

Methods

Experimental Synthesis and Characterization. Na_2LiAlD_6 was synthesized by ball milling $LiAlD_4$ and $2NaAlD_4$ in a Fritsch P7 planetary ball mill with a ball to sample mass ratio of 20 and at 700 rpm for 3 h, followed by heat treatment at 180 °C and 30 bar. All operations were performed under argon in a glove box with less than 1 ppm O_2 and H_2O.

Synchrotron Radiation Powder X-Ray (SR−PXD) data at 110 K were collected at the Swiss-Norwegian beam line (station BM1B) at the European Synchrotron Radiation Facility (ESRF) in Grenoble, France. The samples were kept in rotating 0.5 mm boron-silica-glass capillaries. Intensities were measured in steps of $\Delta(2\theta) = 0.003°$. The wavelength 0.49957 Å was obtained from a channel-cut Si(111) monochromator.

Powder neutron diffraction (PND) data at 8 K were collected with the PUS instrument at the JEEPII reactor at Kjeller, Norway. Neutrons with wavelength 1.5554 Å were obtained from a Ge-(511) focusing monochromator. The detector unit consists of two banks of seven position-sensitive ^3He detectors, each covering 20° in 2θ (binned in steps of 0.05°). Data were collected from 10 to 130° in 2θ. The sample was placed in a rotating cylindrical vanadium sample holder with 5 mm diameter.

Rietveld refinements were carried out using the program Fullprof (version 2.80).[15] X-ray form factors and neutron scattering lengths were taken from the Fullprof library. Pseudo-Voigt profile functions were used, and the backgrounds were modeled by interpolation between manually chosen points.

First-Principles Calculations. Two methodologies were linked for the first-principles prediction of finite temperature thermodynamic properties of the solid-state phases in the Na−Li−Al−H system. These methodologies were detailed in preceding papers on the lower order phases within the Li−Al−H ternary system,[11] the Na−H binary system,[16] and the Na−Al−H ternary system.[12,17] The first methodology employed was a full structure minimization at the ground state using the density functional theory (DFT) implemented in the Vienna Ab initio Simulation Package (VASP) version 4.6 with plane wave basis sets.[18−20] The second methodology generated finite temperature thermodynamic predictions of the minimized structure using the direct method lattice dynamics approach of Parlinski et al.,[21] implemented in the Materials Design Phonon direct method module interfaced with the VASP code[22] (herein referred to as the "Phonon direct method"). This study focused exclusively on the Na_2LiAlH_6 quaternary phase, which was predicted with geometry optimizations to be the only stable quaternary phase to exist within the Na−Li−Al−H system.[8−10] The thermodynamic predictions of lower order stable solid-state compound phases with the Na−Li−Al−H systems $NaAlH_4$, Na_3AlH_6, $LiAlH_4$, Li_3AlH_6, NaH, and LiH have already been reported.[11,12,16] The first-principles thermodynamic property predictions of these phases will be employed to make a comprehensive survey of possible reactions and competitive phase stability within the Na−Li−Al−H system.

(11) Løvvik, O. M.; Opalka, S. M.; Brinks, H. W.; Hauback, B. C. *Phys. Rev. B* **2004**, *69*, 134117/1−9.
(12) Qiu, C.; Opalka, S. M.; Olson, G. B.; Anton, D. L. *Int. J. Mat. Res.* **2006**, *97*, 1484−1494.
(13) Brinks, H. W.; Hauback, B. C.; Srinivasan, S. S.; Jensen, C. M. *J. Phys. Chem. B* **2005**, *109*, 15780−15785.
(14) Tang, X.; Mosher, D. A.; Anton, D. L. In *Materials and Technology for Hydrogen Storage and Generation*; Nazri, G-A., Ping, C., Young, R. C., Nazri, M., Wang, J., Eds: Mater. Res. Soc. Symp. Proc. 884E; Materials Research Society: Warrendale, PA, 2005; p GG4.4.
(15) Rodríguez-Carvajal, J. *Phys. B* **1993**, *192*, 55−69.
(16) Qiu, C.; Opalka, S. M.; Olson, G. B.; Anton, D. L. *Int. J. Mat. Res.* **2006**, *97*, 845−853.
(17) Opalka, S. M.; Anton, D. L. *J. Alloys Comp.* **2003**, *356−357*, 486−489.
(18) Kresse, G.; Hafner, J. *Phys. Rev. B* **1993**, *47*, 558−561.
(19) Kresse, G.; Furthmuller, J. *Comput. Mater. Sci.* **1996**, *6* (1), 15−50.
(20) Kresse, G.; Furthmuller, J. *Phys. Rev. B* **1996**, *54*, 11169−11186.
(21) Parlinski, K.; Li, Z. Q.; Kawazoe, Y. *Phys. Rev. Lett.* **1997**, *78*, 4063−4066.
(22) Parlinski, K. *MedeA-Phonon Version 1.0 using Phonon Software 3.11*; Materials Design, Inc.: Angel Fire, NM.

This study sought to identify the most stable ground state Na_2LiAlH_6 allotrope to input into the Phonon direct method for reliable thermodynamic predictions. The search for the most stable structure followed a structural analog protocol similar to that described in our paper on the Li−Al−H system[11] and in subsequent studies on the bialkali system.[8−10] Here, Na_2LiAlH_6 candidate structures were derived by substitution of ions into stoichiometrically equivalent analogous ternary and quaternary compounds having structures representing the widest possible range of space groups. The VASP minimizations employed the generalized gradient approximation (GGA) of Perdew and Wang,[23] and the valence electrons were explicitly represented with projector augmented wave (PAW) potentials,[24] using the valence configurations: Na $2s^2 2p^6 3s^1$, Li $2s^1$, Al $3s^2 3p^1$ and H $1s^1$. The plane wave cutoff energy of 780 eV and the Gaussian smearing with an energy broadening of 0.2 eV was used. Odd-sized k-point meshes were created by a Monkhorst-Pack scheme for minimization of the primitive cells,[25] using a *k*-mesh spacing of 0.2 $Å^{-1}$ or smaller. The overall total energy convergence error for these parameters was well below 0.01 meV/unit cell. The convergence criterion for electronic self-consistent field convergence was 10^{-7} eV. A full minimization method was employed to allow simultaneous relaxation of ionic coordinates, unit cell size, and shape. The ground state structure was determined by minimizing the Hellmann−Feynman forces with the conjugate gradient algorithm, until all of the ionic forces were less than 0.005 eV/Å. Following convergence, the minimizations were restarted, as necessary, until no further ionic relaxation took place. A final total energy calculation with accurate precision was made using the tetrahedron smearing method with Bloechl corrections.[26]

The Phonon direct method was employed to predict the lattice dynamics using the harmonic approximation on the VASP minimized Na_2LiAlH_6 structures that had the combination of the lowest ground state energy and the highest space group symmetry. Displacements were made on $1 \times 1 \times 1$ supercells for the $Fm\bar{3}m$ and $P4_2/n$ Na_2LiAlH_6 structure (40 atoms each), and on a $2 \times 2 \times 1$ supercell of $P2_1/n$ Na_2LiAlH_6 structure (80 atoms). A 0.1 strength of condition factor was applied for translational invariance. Following the methodology described in the preceding Na−H paper,[16] the integrated predicted phonon density of states was analyzed with statistical mechanical functions to determine the vibrational contribution as a function of temperature. The vibrational contribution was added to the ground state electronic energy, to approximate the Gibbs free energy as a function of temperature, $G(T)$. The finite temperature free energy $G(T)$ values referred to the constitutive stable element 298 K enthalpy values, are called *GHSER* values.[16] Predicted hydride *GHSER* values were used in combination with established values for elemental and gaseous phases[27,28] in the Thermo-Calc program[29] to calculate thermodynamic reaction energies, equilibria, and phase diagrams.

Results and Discussion

A thorough evaluation of the mixed sodium-lithium alanate system for hydrogen storage media required a thermodynamic description of the Na_2LiAlH_6 quaternary phase and the related lower order competing or dissociation phases: $NaAlH_4$, Na_3AlH_6, NaH, LiH, etc. The recently reported dissociation pressure data[4,5] can be used to derive a partial thermodynamic description for the Na_2LiAlH_6 phase, provided that the thermodynamic properties of the other phases in the dissociation reaction are already thermodynamically parametrized. However, the measured or predicted heats of formation and heat capacity properties required for a complete thermodynamic description of the Na_2LiAlH_6 phase have not yet been reported. For this reason, the Na_2LiAlH_6 thermodynamic properties were predicted in this study using the Phonon direct method. It was necessary to identify a stable Na_2LiAlH_6 ground state structure for reliable thermodynamic property predictions. This is because the contributions of the imaginary phonon frequencies generated for metastable ground state phase structures cannot be accounted for, with the present thermodynamic prediction methodology.

Previous refinements of near room-temperature crystallographic analyses of Na_2LiAlH_6/Na_2LiAlD_6 using powder X-ray diffraction (PXD),[2,30] SR−PXD,[3−5] and PND[3] consistently yielded a $Fm\bar{3}m$ ordered perovskite cubic structure with a lattice constant ranging from 7.405 to 7.407 Å. Small imperfections in the SR−PXD data of the cubic (400) reflection may indicate a possible small deviation from cubic symmetry.[3] However, PND data did not give any such indication, and input of lower symmetry structures did not improve upon the quality of the excellent refinement fit made with $Fm\bar{3}m$ structure.[3]

Density functional theory (DFT) simulations did not corroborate the existence of a stable $Fm\bar{3}m$ Na_2LiAlH_6 structure at the ground state. Earlier DFT minimization surveys were made using analog structures representing six different crystallographic types to predict stable global minimum structures for bialkali aluminum hexahydride phases.[8−10] These studies were not able to distinguish between the monoclinic $P2_1/c$ and the cubic $Fm\bar{3}m$ structures for the Na_2LiAlH_6 phase,[8] since the differences in cell parameters and atomic coordinates between the two structures were below the calculation accuracy. However, since the monoclinic structure was slightly more stable than the cubic one, the monoclinic structure was presented in more detail; this also illustrated how the difference between the structures mainly lay in the tilting of the AlH_6 octahedra.

In order to probe the possible existence of lower symmetry Na_2LiAlH_6 structures at temperatures approaching the ground state, additional PND analyses were made at 8 K with the same Na_2LiAlD_6 sample characterized in the recent PND study.[3] The 8 K PND data is shown with the previous 295 K data in Figure 2. The 8 K PND data clearly indicated a reduction of the lattice symmetry, evidenced by the extra reflections and altered intensities of the reflections present in the cubic structure. However, the reflections of the $Fm\bar{3}m$ cubic structure could not be detected to be split. The previously refined Na_2LiAlD_6 structure consists of corner-

(23) Perdew, J. P.; Chevary, J. A.; Vosko, S. H.; Jackson, K. A.; Pederson, M. R.; Singh, D. J.; Fiolhais, C. *Phys. Rev. B* **1992**, *46*, 6671−6687.
(24) Kresse, G.; Joubert, D. *Phys. Rev. B* **1999**, *59*, 1758−1775.
(25) Monkhorst, H. J.; Pack, J. D. *Phys. Rev. B* **1976**, *13*, 5188−5192.
(26) Bloechl, P. E.; Jepsen, O.; Andersen, O. K. *Phys. Rev. B* **1994**, *49*, 16223−16233.
(27) Ansara, I.; Sundman, B. In *Computer Handling and Dissemination of Data*; Glaeser, P. S., Ed.; North-Holland: Amsterdam, 1987; Vol. 1.
(28) Chase, M. W. *NIST-JANAF Thermochemical Tables*, 4th ed.; J. Phys. Chem. Ref. Data, Monograph 9; American Chemical Society and American Institute of Physics: Washington, DC, 1998; pp 1−1951.
(29) Thermo-Calc software, AB. Version Q, Stockholm, Sweden.
(30) Claudy, P.; Bonnetot, B.; Bastide, J. P.; Létoffé, J. M. *Mat. Res. Bull.* **1982**, *17*, 1499−1504.

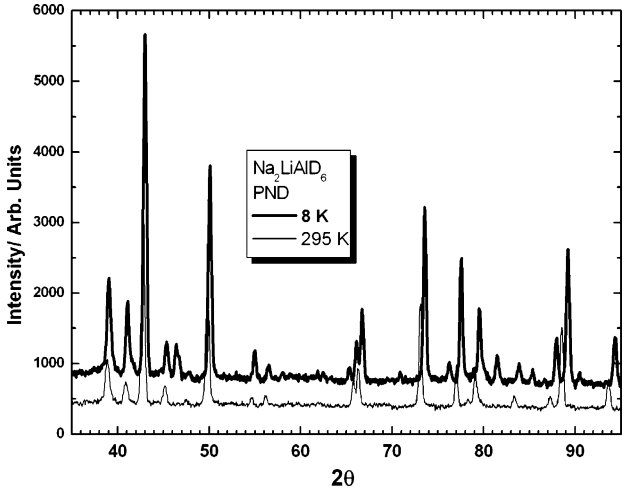

Figure 2. $Na_2LiAlH(D)_6$ powder neutron diffraction (PND) structural analyses at 8 and 295 K.

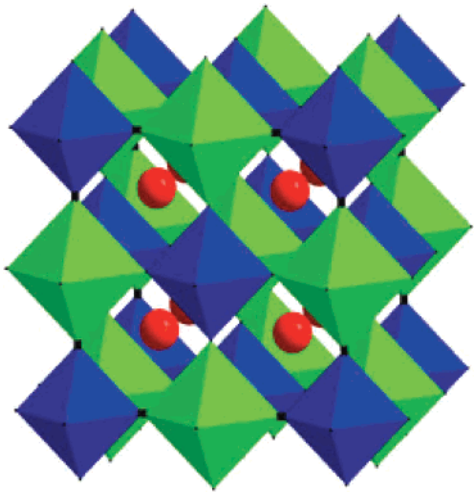

Figure 3. Crystal structure of Na_2LiAlD_6 at room temperature. AlD_6 octahedra (blue) and LiD_6 octahedra (green) form a corner-sharing network where each corner is shared between two octahedra. Na atoms (red) are in interstitial positions surrounded by 12 D atoms.

sharing AlD_6 and LiD_6 octahedra of different sizes, where each D corner is shared between AlD_6 and LiD_6 octahedra, with 180° Al−D−Li bond angles, as shown in Figure 3.[3] These octahedra may be rotated along the three axes and may be tilted in either a positive or negative mode, where adjacent octahedra layers are rotated in the same or opposite direction, respectively. Glazer[31] and later Woodward[32] studied all the different possible tilt systems, both for normal perovskites (ABX_3) and for ordered perovskites ($A_2BB'X_6$). They have given the unit cell size, space group, and approximate atomic positions of the different tilt systems. There are 23 tilt systems with 15 different models. By looking at the unit cell size and extinctions of the space groups, seven of the models were eliminated. The remaining eight models were checked by Rietveld refinements of the PND data, and five turned out to have approximately the same reliability factor χ^2 of 1.98−2.08, as shown in Table 1. The Rietveld fit of one of the models, i.e., model II with

(31) Glazer, A. M. *Acta Cryst. A* **1975**, *31*, 756−762.
(32) Woodward, P. M.; *Acta Cryst. B* **1997**, *53*, 32−43.

Table 1. Best Structural Models Tested for Na_2LiAlD_6 Powder Neutron Diffraction at 8 K[a]

rotation model	space group	χ^2	distance Al-D (Å)	no. atomic parameters
I a^0b^+c-	$C2/c$	2.07	1.768	11
II a^+b-b-	$P2_1/n$	2.08	1.765	12
III a^+a^+c-	$P4_2/n$	2.03	1.763	10
IV a^+b^+c-	$P2/c$	1.98	1.770	22
V a^+b-c-	$P\bar{1}$			48

[a] Models based on ordered perovskite structures from Woodward, 1997, rotation mode according to Glazer, 1975; space group, χ^2, average Al−D distance and number of atomic parameters are given.

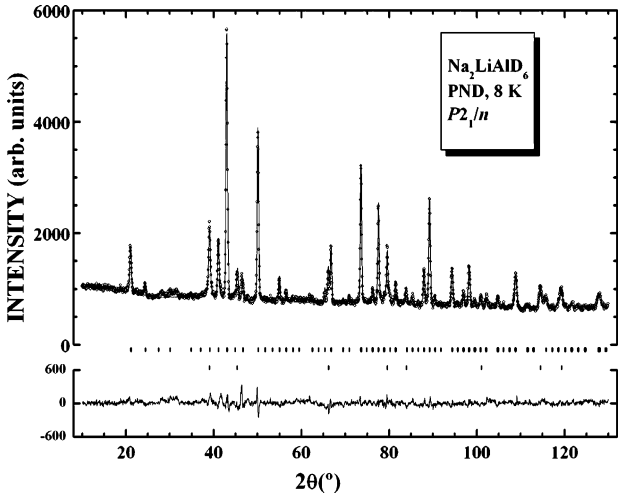

Figure 4. Refinement of 8 K $Na_2LiAlH(D)_6$ structure.

space group $P2_1/n$, is shown in Figure 4. Except for well-known instrumental peaks from the cooling system at 31 and 46°, the fit is acceptable. The last two models have a significantly higher number of refined atomic parameters without achieving the corresponding improvement in the fit and can hence be rejected. Models I−III have the same fit of the PND data, approximately the same number of atomic parameters, and very similar average Al−D distances that are close to the distances at room temperature. From PND measurements it was confirmed that the transition takes place above 110 K. Therefore, SR−PXD data at 110 K was used in an attempt to distinguish between the models. But no splittings of the cubic reflections, i.e., the reflections of the $Fm\bar{3}m$ model, were observed. From PND and SR−PXD, it appeared that Na_2LiAlD_6 at low temperature assumed one of ordered perovskite structures in space group $C2/c$, $P2_1/n$, or $P4_2/n$ described by Woodward,[32] but it was not possible to conclude which one best described the crystal structure.

The first three tilt structures that gave the best refinement fits (cf. Table 1) were reviewed to prepare for Phonon direct method lattice dynamic simulations. First, full ground state minimizations were made of the newly identified C_2/c and $P2_1/n$ monoclinic structures, and the $P4_2/n$ tetragonal structures. The energies and the structural properties are compared to the previous results calculated for the $P2_1/c$, $Fm\bar{3}m$, and $Immm$ structure types[8] in Table 2. The $P2_1/n$ structure is related to the previously determined $P2_1/c$ structure, where each structure corresponds to a different unit cell representation of space group no. 14. It can be seen that with the exception of the $Fm\bar{3}m$ and $Immm$ structures, the energies

Table 2. Ground State Minimized Na_2LiAlH_6 Candidate Structures

space group	electronic energy (kJ mol^{-1} atom^{-1})	lattice paramete rs				volume (Å^3/atom)
		a (Å)	*b* (Å)	*c* (Å)	*β* (deg)	
Immm	−289.2	5.405	5.410	7.647		11.16[a]
$Fm\bar{3}m$	−300.2	7.338	7.338	7.338		9.88[a]
C_2/c	−300.5	7.325	7.371	7.359	90.01	9.89
$P4_2/n$	−300.5	7.356	7.356	7.370		9.97
$P2_1/n$	−300.6	5.194	5.208	9.006	125.20	9.95
$P2_1/c$	−300.6	5.165	5.251	7.339	90.03	9.95[a]

[a] Reference 8.

are very close to one another and are not distinguishable within the limits of accuracy for VASP ground state calculations. These results can be interpreted to imply that there may be a number of energetically equivalent crystal structures accessible at the ground state.

Phonon direct method lattice dynamic predictions were made on the highest symmetry $Fm\bar{3}m$, $P4_2/n$, and $P2_1/n$ minimized structures. This enabled the comparison of the phonon dispersion relations of the original refined $Fm\bar{3}m$ structure with two of the most stable, energetically equivalent simulated structures. The phonon dispersion relations for the $Fm\bar{3}m$ and $P2_1/n$ phases are shown in Figure 5a−b. Both the $Fm\bar{3}m$ and the $P4_2/n$ dispersion relations exhibited significant imaginary frequencies representing instabilities to transformation to other phase structures. The $Fm\bar{3}m$ structure dispersion had an unstable T_{1g} acoustical mode at the γ point. The $P4_2/n$ structure had two imaginary B_g and A_g Raman-active branches. The $P2_1/n$ structure lacked imaginary dispersion frequencies and was hypothesized to be the most stable ground state phase.

These observations brought forth to question the relationship between the predicted stable $P2_1/n$ ground state structure and the experimentally observed $Fm\bar{3}m$ room-temperature structure. The first scenario postulated was that the $Fm\bar{3}m$ structure could undergo one or more second-order transformations with decreasing temperature to form the $P2_1/n$ structure. One possible pathway could be a multistep transformation of $Fm\bar{3}m$ to $P4_2/n$ structure, followed by transformation to the $P2_1/n$ structure. However, animation with the Medea Phonon module of the $Fm\bar{3}m$ instability at the Γ point led to a $P\bar{1}$ structure. Likewise, animation of the instabilities at the *W*, *X*, *K*, and *L* points led to a structures in the space groups *P*2, *P*4/*nmc*, *Pm*, and *R*3, respectively. Following an established approach for the investigation of phase transformations,[33] the Bilbao Crystallographic Server Subgroupgraph program[34] was used to determine whether the *P*2, *P*4/*mnc*, *Pm*, and *R*3 spacegroups and other spacegroups could be intermediate subgroups between the $Fm\bar{3}m$ spacegroup and the $P2_1/n$, $C2/c$, or $P4_2/n$ structures. Indeed, such a direct transformation pathway was found between the $Fm\bar{3}m$ and the $P2_1/n$ and $C2/c$ structures; this is illustrated in Figure 6. The figure shows that $Fm\bar{3}m$ is connected to both the monoclinic $P2_1/n$ and $C2/c$ structures via the *X* instability, through the *P*4/*mnc* structure. This means that

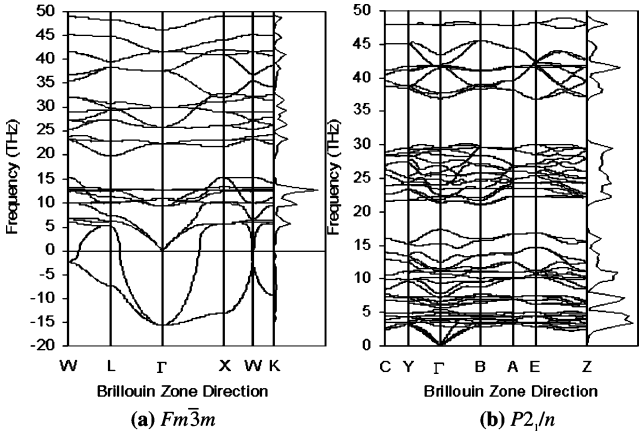

Figure 5. Phonon dispersion plots for the Na_2LiAlH_6 (a) $Fm\bar{3}m$ and (b) $P2_1/n$ structures.

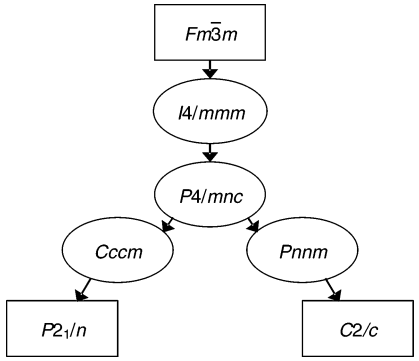

Figure 6. The maximal group-subgroup relations connecting the cubic $Fm\bar{3}m$ structure with the monoclinic $P2_1/n$ and $C2/c$ structures through the *P*4/*mnc* structure, which is the result of an instability of the $Fm\bar{3}m$ structure at the *X* point.

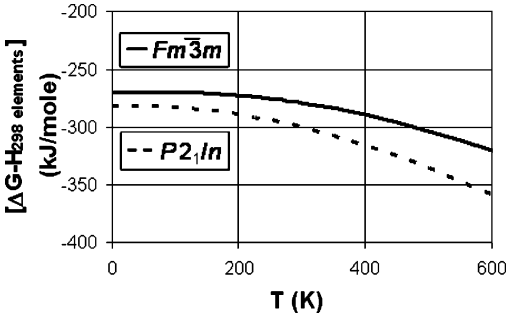

Figure 7. Thermodynamic predictions determined from direct method lattice vibrational calculations.

these monoclinic structures are closely related to the instability of the cubic structure, which may explain why the latter is not stable at low temperatures.

The predicted *GHSER* values for the $P2_1/n$ Na_2LiAlH_6 phase are compared to those for the $Fm\bar{3}m$ phase in Figure 7, where only the integrated phonon density of state values over frequencies ≥0 were used to predict the $Fm\bar{3}m$ phase thermodynamic values. The $P2_1/n$ phase was predicted to be significantly more stable than the $Fm\bar{3}m$ phase at all temperatures. A crossover in the *GHSER* values, which would indicate a transformation from the $P2_1/n$ phase to the $Fm\bar{3}m$ phase with increasing temperature, was not predicted. A second simpler scenario relating the phase structures is even more credible. The $P2_1/n$ and other simple tilt structures

(33) Perez-Mato, J. M.; Aroyo, M.; García, A.; Blaha, P.; Schwarz, K., Schweifer, J.; Parlinski, K. *Phys. Rev. B* **2004**, *70*, 214111/1−14.
(34) Ivantchev, S.; Kroumova, E.; Madariaga, G.; Perez-Mato, J. M.; Aroyo, M. I. *J. Appl. Cryst.* **2000**, *33*, 1190−1191.

Table 3. Summary of Reported $Na_2LiAlH(D)_6$ Mechanochemical Syntheses

reactants	anneal T (K)	anneal P (bar)
$LiH + 2NaH + AlH_3$[a]	373	200
$LiAlD_4 + 2NaH$[b]	423	50
$LiAlH_4 + 2NaH$[c]	–	–
$LiH + NaH + NaAlH_4$[d]	–	–
$LiH + NaH + NaAlH_4$[c]	–	–
$LiAlD_4 + 2NaAlD_4$[b]	453	30
$LiH + 2NaAlH_4$[e]	453	80

[a] Reference 35. [b] Reference 3. [c] Reference 5. [d] Reference 2. [e] Reference 4.

could be actually comprised of two (or more) mirror-symmetry equivalent structures, each where the AlH_6 octahedra are tilted off-center from the $Fm\bar{3}m$ cubic structure in opposite directions. With the availability of kinetic energy with increasing temperature, the energy barriers to tilting could be overcome, and the octahedra could rapidly tautomerize between these equivalent structures. During the crystallographic analyses at elevated temperatures, these equivalent oscillations could be time-averaged to appear as the intermediate cubic structure. In order to explore this possible phenomenon, the $Fm\bar{3}m$ structure was recast in $P2_1/n$ symmetry, and a tilting pathway with three intermediate steps was constructed between the two structures. By recasting the $Fm\bar{3}m$ structure in the $P2_1/n$ symmetry, the unit cell and atom positions were as similar as possible to the $P2_1/n$ structure. This gave an almost perfect cancellation of any systematic errors in the calculations of structures along the pathway, yielding accurate relative energies. The total energy calculated for each step along the tilting pathway showed a progressive increase with no intermediate barriers, starting from the $P2_1/n$ and ending with the $Fm\bar{3}m$ structure. To oscillate from one $P2_1/n$ structure to the mirror symmetry equivalent structure, the octahedra would have to pass through a ground state intermediate cubic barrier of 0.4 kJ mol^{-1} $atom^{-1}$, the difference in energy between the $P2_1/n$ and $Fm\bar{3}m$ structures. Any thermal energy or even the zero-point vibrational energy would be sufficient to overcome this barrier, as mentioned above, so for such a small barrier the structure can be characterized as the average of the tautomers, which is the $Fm\bar{3}m$ structure. The structure at any reasonable temperature may actually be the tautomer average of a number of energetically similar structures that represent different tilting of the AlH_6 octahedra (such as the most favorable structures listed in Table 2).

Thermodynamic descriptions generated from the Phonon direct method were used to evaluate compound formation and dissociation reactions within the Na−Li−Al−H system. The various mechanochemical routes reported in the literature for the synthesis of the Na_2LiAlH_6 phase[2−5,35] are summarized in Table 3. Many of these syntheses used annealing treatments to increase the detectable yield of Na_2LiAlH_6. The

(35) Anton, D. L.; Opalka, S. M. VI.A.4 *Complex Hydride Compounds with Enhanced Hydrogen Storage Capacity*; DOE Hydrogen Program 2005 Annual Progress Report; U.S. Department of Energy: Washington, DC, 2005 (http://www.hydrogen.energy.gov/pdfs/progress05/vi_a_4_anton.pdf).

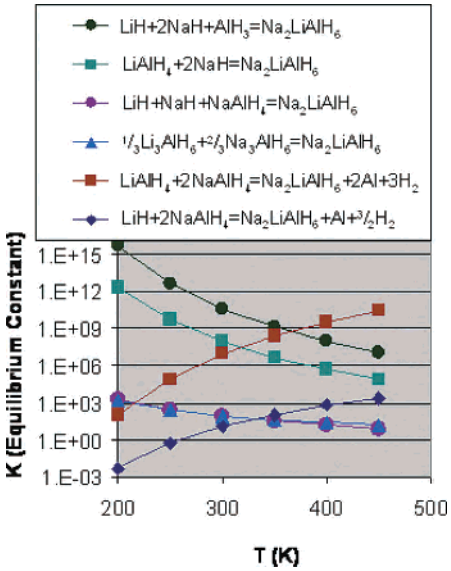

Figure 8. Predicted Na_2LiAlH_6 synthesis reactions.

predicted thermochemical equilibrium constants, K_{eq}, for the related Na_2LiAlH_6 synthetic reactions versus temperature

$$LiH + 2NaH + AlH_3 = Na_2LiAlH_6 \quad (1)$$

$$LiAlH_4 + 2NaH = Na_2LiAlH_6 \quad (2)$$

$$LiH + NaH + NaAlH_4 = Na_2LiAlH_6 \quad (3)$$

$$1/3Li_3AlH_6 + 2/3Na_3AlH_6 = Na_2LiAlH_6 \quad (4)$$

$$LiAlH_4 + 2NaAlH_4 = Na_2LiAlH_6 + 2Al + 3H_2 \quad (5)$$

$$LiH + 2NaAlH_4 = Na_2LiAlH_6 + Al + 3/2H_2 \quad (6)$$

are plotted in Figure 8. The higher the K_{eq}, the greater the reaction equilibrium shifts to the products. As expected, in reactions 1 and 2 with the metastable AlH_3 and $LiAlH_4$ precursors were predicted to have a greater Na_2LiAlH_6 yield. However, the K_{eq} for these reactions decreases with increasing temperature, and reaction 5 is predicted to predominate at temperatures greater than ~373 K (~100 °C). These predictions show why the reaction 5 using $NaAlH_4$ and $LiAlH_4$ precursors employed by Brinks et al.[3] required a 453 K anneal to increase the Na_2LiAlH_6 fraction. These results demonstrate the potency of the predictive thermodynamic methodology for designing the best experimental conditions for synthesis of a target phase.

The thermochemical predictions provided insight into how various possible dissociation mechanisms may be interrelated with changing temperature. Hydride dissociation reactions are commonly described in terms of reaction dissociation enthalpies, ΔH_{dis}, determined from the slope of the Arrhenius plot of the equilibrium H_2 pressure formed upon dissociation versus the reciprocal of the equilibrium temperature, according to the van't Hoff equation: $\ln P_{H2} = \Delta H_{dis}/RT + \Delta S/R$, where P is the equilibrium H_2 pressure at temperature T, S in the dissociation entropy, and R is the universal gas constant. The predicted ΔH_{dis} for Na_2LiAlH_6 and Na_3AlH_6 dissociation reactions per dissociation of 1 mole H_2

$$2/3Na_2LiAlH_6 = 4/3NaH + 2/3LiH + 2/3Al + H_2 \quad (7)$$

$$2/3Na_3AlH_6 = 2NaH + 2/3Al + H_2 \quad (8)$$

are compared to ΔH_{dis} values determined from pressure composition isotherm measurements[4,5,36] in Table 4. The predicted ΔH_{dis} values were smaller, but were within 10 kJ/mol of the reported measured equilibrium values. A residual error of up to10 kJ/mol in the predicted ΔH_{dis} can impact the predicted dissociation pressure by a factor of up to 25 at 373 K.

The differences between the predicted and measured values were most likely due to the inherent inaccuracies in the ground state minimizations with the density functional exchange-correlation GGA approximation, and/or the harmonic approximation which does not account for the possible anharmonic free rotational modes of the AlH_6 octahedra. Such rotations would be described by 3 of the 27 total degrees of freedom in the Na_2LiAlH_6 structures, and thus affect a relatively small proportion of the vibrational thermodynamic contributions. An upper bound to the error from using the harmonic approximation for the rotations of the AlH_6 groups is given by assuming that they are free rotors and comparing the thermodynamic functions to those calculated for the approximately 3 THz harmonic oscillators from the harmonic approximation. The error in the enthalpy and free energy is no more than 6 kJ/mol over the temperature range considered. This is an upper bound and the actual error due to the harmonic approximation is probably considerably less.

The van't Hoff plot for the most favorable predicted dissocation reactions are shown in Figure 9, in terms of equivalent starting amount of Na_2LiAlH_6 (not per equivalent mole of H_2 generated), for ease of comparison. The expected dehydrogenation reaction to form binary hydrides, aluminum and 3.5 wt. % H_2 [reaction 7], is predicted to be favorable at temperatures above 360 K (87 °C). The predicted dissociation curve traverses the lower left-hand corner of the window of reversibility, generating a lower dissociation pressure with respect to the dissociation reaction for the equivalent amount of Na_3AlH_6 (the comparison can be made by referring to Table 4). At temperatures below 360 K, a higher dissociation H_2 pressure and hence greater favorability is predicted for the reaction

$$2/3Na_2LiAlH_6 = 4/9Na_3AlH_6 + 2/3LiH + 2/9Al + 1/3H_2 \quad (9)$$

which releases only 1.2 wt. % H_2.

Experimental observations corroborated the predicted relationship between the competing Na_2LiAlH_6 dissociation reactions 7 and 9. In situ PXD showed that for Ti-enhanced Na_2LiAlH_6 heated in vacuum at 1 K/min, Na_2LiAlH_6 was partially dissociated via Na_3AlH_6 before Na_2LiAlH_6 was thermally dissociated to NaH, LiH and Al. The Na_3AlH_6 formed was dissociated before the remaining Na_2LiAlH_6 reacted. The same effect was seen, but too less degree, with pure Na_2LiAlH_6: Traces of Na_3AlH_6 were seen in the diffraction diagrams at intermediate temperatures below the main dissociation of Na_2LiAlH_6. This proved experimentally that at lower temperature, Na_3AlH_6 was more stable than Na_2LiAlH_6, whereas at higher temperature Na_3AlH_6 was less stable than Na_2LiAlH_6. In addition, it showed that the metal ions had sufficient mobility for such a reaction to take place at relatively low temperature.

Table 4. Comparison of Predicted and Measured Dissociation Energies

dissociation enthalpy ΔH_{dis} (kJ/mol)	
predicted	measured
$2/3Na_2LiAlH_6 => 4/3NaH + 2/3LiH + 2/3Al + H_2$	
47.5	56.4[a]
	53.5[b]
$2/3Na_3AlH_6 => 2NaH + 2/3Al + H_2$	
44.8	47[c]

[a] Reference 4. [b] Reference 5. [c] Ref 36.

Phase diagram predictions were made to assess the relative stability of the different phases in the quaternary Na−Li−Al−H system with composition, temperature, and pressure. An excellent perspective was obtained from Na−Li−Al ternary sections calculated at constant H_2 activity, temperature, and pressure. Ternary sections generated with the fixed conditions (a) 100 bar, 300 K (27 °C), and 3.9×10^{-3} H_2 activity and (b) 100 bar, 400 K (127 °C), and 1.0×10^{-3} H_2 activity are shown in Figure 10a,b. The lines in these diagrams demarcate the regions where common sets of phases coexist. The Na_2LiAlH_6 phase is shown to coexist with the ternary alanate and the elemental hydride phases is predicted over a wide compositional range in these diagrams.

The phase equilibria were systematically surveyed over varying conditions to identify the composition, temperature, and pressure conditions for the optimum reversible hydrogen retrieval in the Na−Li−Al−H system. The optimum composition contained the elemental stoichiometry: {2 Na:1 Li:2

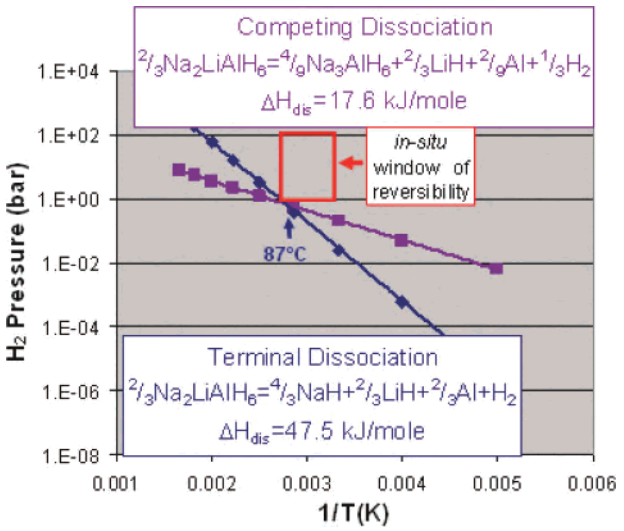

Figure 9. Predicted van't Hoff plot for most favorable Na_2LiAlH_6 dissociation reactions, compared for equivalent starting amount of Na_2LiAlH_6. The in situ window of reversibility is defined by the practical 1−100 bar pressure range and 25−100 °C temperature range for hydrogen storage system operation.

(36) Bogdanovic, B.; Brand, R. A.; Marjanovic, A.; Schwickardi, M.; Tolle, J. *J. Alloys Comp.* **2000**, *302*, 36−58.

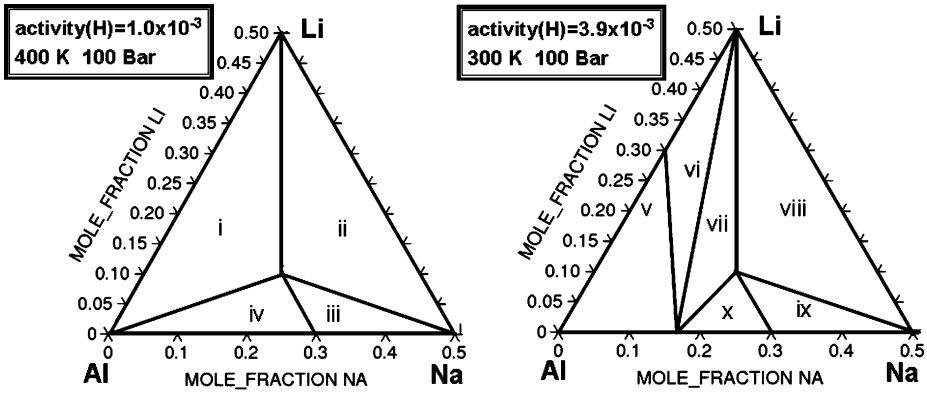

(a) 300 K (27°C) and 3.9×10^{-3} H_2 activity **(b)** 400 K (127°C) and 1.0×10^{-3} H_2 activity

Figure 10. Na−Li−Al ternary sections from thermodynamic property predictions (a) at 100 bar, 300 K and 3.9×10^{-3} H_2 activity with phase mixture regions (i) Al, LiH, Na_2LiAlH_6, (ii) NaH, LiH, Na_2LiAlH_6, (iii) NaH, Na_3AlH_6, Na_2LiAlH_6, and (iv) Al, Na_3AlH_6, Na_2LiAlH_6 and (b) at 100 bar, 400 K (127 °C) and 1.0×10^{-3} H_2 activity with phase mixture regions (v) Al, $NaAlH_4$, Li_3AlH_6, (vi) LiH, $NaAlH_4$, Li_3AlH_6, (vii) LiH, $NaAlH_4$, Na_2LiAlH_6, (viii) LiH, NaH, Na_2LiAlH_6, (ix) NaH, Na_3AlH_6, Na_2LiAlH_6, and (x) $NaAlH_4$, Na_3AlH_6, Na_2LiAlH_6.

Al:9 H}. Under the conditions of 300 K and 100 bar, this composition is predicted to form fully hydrided $NaAlH_4$ and LiH phases, in a ratio of 2:1. The predictions show that LiH destabilizes the dissociation of $NaAlH_4$ to form the more favorable Na_2LiAlH_6 phase [reaction 6], increasing the H_2 plateau pressure approximately 1 order of magnitude to 11 bar at 306 K (33 °C) compared to the first dissociation reaction of pure $NaAlH_4$[36]

$$NaAlH_4 = 1/3Na_3AlH_6 + 2/3Al + H_2 \qquad (10)$$

However, the benefits for destabilization are compromised by the extra weight of LiH which dilutes the total capacity of $NaAlH_4$, and the smaller amount of H_2 released in the first dissociation step: 2.6 wt. % H_2 for reaction 6 versus 3.7 wt. % H_2 for reaction 10. At temperatures higher than 360 K at 1 bar pressure, the dissociation of the Na_2LiAlH_6 phase [reaction 7] has a greater equilibrium constant than the dissociation of the equivalent amount of pure Na_3AlH_6 [reaction 8]. The amount of hydrogen released is greater in the Na_2LiAlH_6 decomposition reaction, 2.6 wt. % H_2, compared to that released in the second Na_3AlH_6 dissociation reaction, 1.9 wt. % H_2. It is envisioned that the two step dissociation process could be used to extract 5.2 wt. % H_2 reversibly from the optimum {2 Na:1 Li:2 Al:9 H} composition: first, degassing through reaction 6 by changing the pressure from 100 to 1 bar at room temperature, and second, degassing through reaction 7 by increasing the temperature to ≥400 K at 1 bar pressure. This reaction pathway is summarized schematically in Figure 11. In practice, often even higher temperatures and/or lower pressures are required to overcome kinetic barriers and to achieve acceptable hydrogen discharge rates. The feasibility of the forward reaction scheme has been experimentally confirmed in recent synthetic studies;[35] however, the reversibility and kinetics of these coupled reactions await further experimental examination.

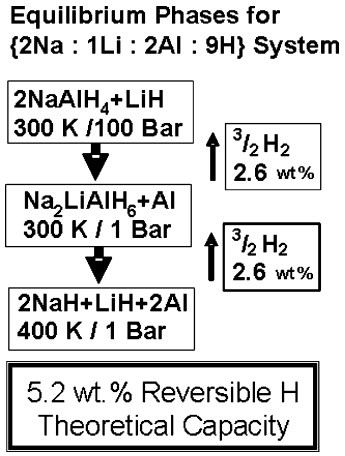

Figure 11. Reaction schematic for maximum theoretical H reversibility in Na−Li−Al−H system.

Conclusion

Combined experimental and theoretical methodologies were used to investigate the structure and transformation behavior of the Na_2LiAlH_6 phase. A low-temperature $P2_1/n$ monoclinic structure was jointly identified through crystallographic refinement and direct method lattice dynamics to be a suitable stable ground state structure for thermodynamic property predictions. Two feasible transformation pathways were proposed to relate this structure to the less stable room temperature observed $Fm\bar{3}m$ structure. First, the $Fm\bar{3}m$ structure may directly transform to the $P2_1/n$ structure along the X instability, passing through an intermediate $P4/mnc$ structure. Second, the $Fm\bar{3}m$ structure could actually be the time-average of a structure that rapidly oscillates between one or more pairs of mirror-symmetry perovskite distortions, formed by tilting of the AlH_6 octahedra. The thermodynamic predictions enabled the thermodynamic modeling of the Na_2LiAlH_6 syntheses and dehydrogenation reactions, generating unique insights into competing reaction mechanisms. The calculated bialkali dissociation pressure relationships were compared with those determined from pressure-composition-isotherm experiments to validate the predicted thermodynamic properties. The predictions of varying Na_2LiAlH_6 dehydrogenation behavior with temperature were substantiated by experimental observations and were used to aid in their interpretation. Gibbs energy minimization and phase diagram predictions were then used to determine the reaction

pathways for the maximum theoretical capacity of 5.2 wt. % H_2 that could be achieved with the Na−Li−Al−H system.

Acknowledgment. S. M. Opalka acknowledges support by the U.S. Department of Energy Contract DE-FC04-02AL67610, and team members: X. Tang, D. A. Mosher, and B. L. Laube and former project leader D. L. Anton. O. M. Løvvik acknowledges support from the Norwegian Research Council through the Nanomat program. The original integrated experimental-theoretical Na−Li−Al−H thermodynamics were generated in collaboration with C. Qiu and G. B. Olson of QuesTek Innovations, LLC. The skillful assistance from the project team at the Swiss−Norwegian beam line, ESRF, is also gratefully acknowledged.

IC062032E